Electrocatalysis

International Edition: DOI: 10.1002/anie.201903290
German Edition: DOI: 10.1002/ange.201903290

Synergy between Plasmonic and Electrocatalytic Activation of Methanol Oxidation on Palladium–Silver Alloy Nanotubes

Lin Huang, Jiasui Zou, Jin-Yu Ye, Zhi-You Zhou, Zhang Lin, Xiongwu Kang, Prashant K. Jain,* and Shaowei Chen*

Abstract: *Localized surface plasmon resonance (LSPR) excitation of noble metal nanoparticles has been shown to accelerate and drive photochemical reactions. Here, LSPR excitation is shown to enhance the electrocatalysis of a fuel-cell-relevant reaction. The electrocatalyst consists of Pd_xAg alloy nanotubes (NTs), which combine the catalytic activity of Pd toward the methanol oxidation reaction (MOR) and the visible-light plasmonic response of Ag. The alloy electrocatalyst exhibits enhanced MOR activity under LSPR excitation with significantly higher current densities and a shift to more positive potentials. The modulation of MOR activity is ascribed primarily to hot holes generated by LSPR excitation of the Pd_xAg NTs.*

Localized surface plasmon resonances (LSPRs) of metal nanoparticles (NPs) allow the strong coupling of visible light with charge carriers in the NP. Energetic charge carriers produced by LSPR excitation of metal NPs catalyze chemical transformations on the surface of the NPs[1–4] and enable light harvesting.[5] Here, we uncover how LSPR excitation of charge carriers in a plasmonic electrocatalyst accelerates a fuel-cell reaction.

Direct methanol fuel cells, while critical for realizing electric vehicles, are difficult to commercialize owing to two limitations of the electrocatalyst: 1) the low catalytic activity for the cathodic oxygen reduction reaction and the anodic methanol oxidation reaction (MOR), and 2) the high cost of the precious-metal-based catalyst.[6] It is desirable to improve the catalytic activity and/or to reduce the use of expensive precious metals in the catalyst. Visible-light excitation of a plasmonic metal nanostructure-based electrocatalyst has been shown to promote the MOR.[7] Herein, we investigate the manner in which LSPR excitation enhances the activity of a electrocatalyst toward MOR. For the study, we developed a plasmonic electrocatalyst consisting of Pd_xAg alloy nanotubes (NTs), which combine the electrocatalytic MOR activity of Pd and the visible-light LSPR absorption of Ag. The alloy electrocatalyst exhibits enhanced current densities under LSPR excitation. Although photothermal heating of the electrochemical interface contributes to the enhancement, the primary mechanism involves hot holes (h^+) generated in the alloy by plasmonic excitation. These hot h^+ drive methanol oxidation, forming a pathway complementary to electro-oxidation.

Pd was chosen as a component of the electrocatalyst not only because of its MOR activity but also its relative resistance against poisoning by CO, a common issue with Pt.[8] Pd and Ag are fcc metals with close lattice constants, so their alloying is favorable over a range of compositions.[9] Four different alloys were prepared, the elemental compositions of which were found by inductively coupled plasma-atomic emission spectroscopy (ICP-AES) to be $x = 0.65$, 0.52, 0.41, and 0.33, where x is the molar ratio of Pd to Ag. The surface composition, however, is less Pd-rich than the overall composition (Supporting Information, Table S1). $Pd_{0.65}Ag$ and $Pd_{0.52}Ag$ alloy NTs were characterized (Supporting Information, Figure S1) by transmission electron microscopy (TEM), elemental mapping, and X-ray diffraction (XRD). The NTs were found to exhibit hollow morphologies, which are desirable from the point-of-view of high specific surface areas. High-resolution X-ray photoelectron spectra (XPS) of the Pd_xAg NTs (Supporting Information, Figure S2) are consistent with alloying.[9,10]

The Pd_xAg NTs were supported on carbon nanotubes (CNTs). The electrocatalytic activity of Pd_xAg/CNTs toward MOR was measured by cyclic voltammetry (CV) in a conventional three-electrode setup in a home-made quartz cell equipped with a cooling bath. The mass activities of $Pd_{0.65}Ag$/CNTs, $Pd_{0.52}Ag$/CNTs, and $Pd_{0.41}Ag$/CNTs were measured to be 0.99, 1.38, and 0.84 A mg^{-1} Pd, respectively, while $Pd_{0.33}Ag$, surprisingly, showed little to no MOR activity (Supporting Information, Figure S3). This dependence of the intrinsic (Pd content-normalized) MOR activity of Pd_xAg alloy NTs on the relative content of Pd and Ag may be a reflection of differences in active site geometry[11] and third-body effects between the alloys. The intermediate $Pd_{0.52}Ag$ composition emerges to be most optimal, in line with the volcano-type

[*] L. Huang, J. Zou, Prof. Dr. Z. Lin, Prof. Dr. X. Kang
School of Environment and Energy
South China University of Technology
Guangzhou 510006 (P. R. China)
E-mail: esxkang@scut.edu.cn
Dr. J.-Y. Ye, Prof. Dr. Z.-Y. Zhou
College of Chemistry and Chemical Engineering, Xiamen University
Xiamen 361005 (P. R. China)
Prof. Dr. P. K. Jain
Department of Chemistry and Materials Research Laboratory
Beckman Institute of Advanced Science and Technology
University of Illinois Urbana-Champaign
Urbana, IL 61801 (USA)
E-mail: jain@illinois.edu
Prof. Dr. S. Chen
Department of Chemistry and Biochemistry
University of California
Santa Cruz, CA 90095 (USA)
Supporting information and the ORCID identification number(s) for the author(s) of this article can be found under: https://doi.org/10.1002/anie.201903290.

dependence of the catalytic activity of alloy nanoparticles on the composition.[11]

Next, the electrocatalytic performance of Pd_xAg/CNTs toward MOR was tested (Figure 1) under visible-light irradiation. Broadband visible-light of wavelengths longer than 400 nm from a Xe lamp was used for photoexcitation. The

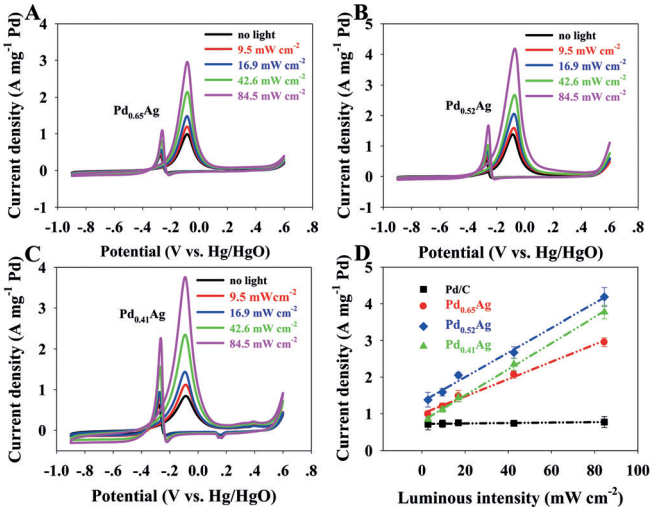

Figure 1. CV scans of CNT-supported A) $Pd_{0.65}Ag$, B) $Pd_{0.52}Ag$, and C) $Pd_{0.41}Ag$ electrocatalysts in an aqueous solution of 1.0 M CH_3OH and 0.5 M NaOH under illumination of white light of different intensities. The CV scan rate was 50 mV s^{-1}. D) Mass activity of Pd/C and Pd_xAg/CNTs (x = 0.65, 0.52, and 0.41) electrocatalysts in MOR as a function of the incident light intensity. Data points in (D) represent the average of measurements from three identical trials, the standard deviation of which is represented by the error bars. Dashed-dotted lines in (D) represent linear fits of these data points.

Pd/C showed negligible enhancement upon illumination, which is consistent with the fact that Pd NPs, smaller than 10 nm in size, have no LSPR absorption in the spectral range of 300–1500 nm.[12] Despite their strong LSPR absorption, Ag nanowires were not active toward MOR in the dark. Consistently no photo-enhanced activity was observed. Thus, photo-enhanced activity toward MOR is displayed only by nanostructures that possess both native electrocatalytic activity due to the Pd component and the ability to harvest light via LSPR excitations due to the Ag component.

The Pd_xAg NTs exhibit LSPR absorption peaking in the 350–400 nm range. The enhanced current density measured for $Pd_{0.52}Ag$ NTs as a function of the excitation wavelength shows a peaked behavior similar to the light absorption response of the NTs (Figure 2 A), as expected for a photo-

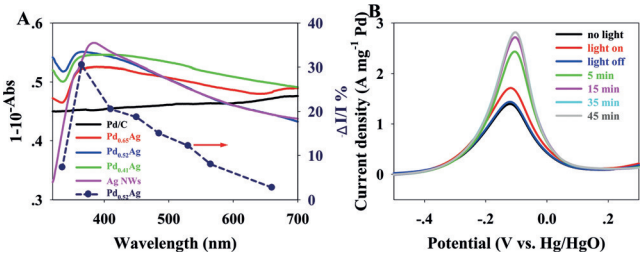

Figure 2. A) Absorbance spectra (solids lines) of aqueous colloids of Pd/C, Ag nanowires, and Pd_xAg (x = 0.65, 0.52, and 0.41) NTs, plotted in the form of the absorbed light intensity fraction, 1–10^{-Abs} (left axis). Alongside, the dark blue dots joined by the dotted blue line show the wavelength dependence of the % enhancement ($\Delta I/I$*100, right axis) in the mass activity of $Pd_{0.52}Ag$/CNTs resulting from light of 15 mW cm^{-2} intensity. B) Mass activity in MOR of $Pd_{0.52}Ag$/CNTs in an aqueous solution of 1.0 M CH_3OH and 0.5 M NaOH at 30 °C under various visible-light (42.6 mW cm^{-2}) illumination conditions.

temperature of the electrolyte system was maintained by a temperature bath at 30 °C over the course of illumination and measurement. $Pd_{0.65}Ag$/CNTs, $Pd_{0.52}Ag$/CNTs, and $Pd_{0.41}Ag$/CNTs showed enhanced mass activity toward MOR under visible-light illumination as compared to the activity in the dark. The activity increased linearly as a function of the incident light intensity (Figure 1 D). The magnitude of light-excitation-induced enhancement of the MOR activity of Pd_xAg/CNTs depended on the molar ratio of Pd to Ag. Among the three active alloys, $Pd_{0.41}Ag$ displayed the poorest activity in the dark; however, this alloy showed the largest enhancement in activity upon light excitation. On the other hand, $Pd_{0.52}Ag$ was the most active catalyst in the dark, but the light-induced enhancement in catalytic activity it exhibited was in-between those of $Pd_{0.41}Ag$ and $Pd_{0.65}Ag$. The trends in the MOR activity of Pd_xAg/CNTs in the dark and under visible-light illumination were consistent with the trends in their charge transfer resistances measured by electrochemical impedance (Supporting Information, Figure S4).

The catalytic activity of Pd/C and Ag nanowires/CNTs toward MOR was also examined both in the dark and under illumination of visible-light of an intensity of 84.5 mW cm^{-2} (Supporting Information, Figure S5). The MOR activity of enhanced process. The photo-enhancement can originate from a photothermal effect and/or photogenerated electrons (e^-) and h^+ resulting from LSPR excitation, as shown instructively by Fang and co-workers[7e] and others.[13] LSPR excitations decay via 10–100-fs timescale e^-–e^- scattering producing energetic e^-–h^+ pairs.[14] These charge carriers can modulate the nature and kinetics of electrochemical reactions occurring at the interface. The photoexcited carriers relax via 1 ps timescale e^-–phonon coupling, resulting in heating of the metal lattice, followed by 100 ps timescale transfer of heat to the surrounding medium.[15] Although a cooling bath maintained the temperature of the bulk electrolyte at 30 °C, limits in the kinetics of heat removal can result in a spatial temperature profile, whereby the electrocatalyst/electrolyte interface may be at an elevated temperature. Consequently, the diffusion of reactive species[13b] and kinetics of electrochemical reactions at the interface may be enhanced by such photothermal heating, potentially resulting in the increase in activity upon visible-light illumination.

The photo-enhancement is reversible but it is not instantaneous. It took minutes after the light-excitation was introduced for the MOR activity of $Pd_{0.52}Ag$/CNTs to stabilize (Figure 2 B). The minutes-scale response to LSPR excitation may be reflective of a gradual approach of the photoinduced

surface temperature and/or surface photopotential to a steady-state value.

To determine if the observed photo-enhancement in the current density is simply due to a photothermal effect, we compared the effect of light illumination on the MOR activity of $Pd_{0.52}Ag$/CNTs with that of an increase in the electrolyte temperature (Figure 3).[16] Under monochromatic 530 nm laser illumination (Figure 3A), the peak current density increased with increasing excitation intensity in a super-linear fashion (Figure 3D). Alongside, the peak potential progressively shifted to the positive direction. An increase in the temperature of the electrolyte under dark conditions did not reproduce the latter effect of light illumination; only the peak current density increased (Figure 3B). The peak potential remained unchanged (Figure 3C). Thus, a photothermally induced temperature rise does not fully account for the enhanced electrocatalytic activity under visible-light excitation. A non-thermal effect is at play.[2]

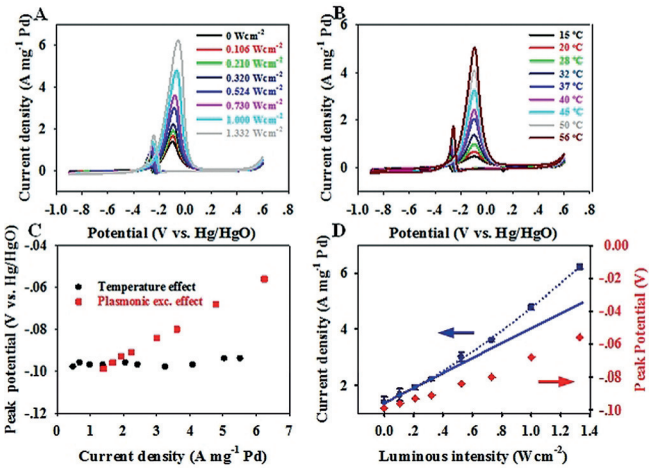

Figure 3. CV scans of $Pd_{0.52}Ag$/CNTs electrocatalyst in an aqueous solution of 1.0 M CH_3OH and 0.5 M NaOH (A) under illumination of various intensities of a 530 nm laser and (B) at different temperatures in the dark. The current densities are normalized to unit mass of Pd. As seen from the vertical lines, meant as visual guides, the peak potential shifts in the positive direction with increasing light intensity in (A), but there is no such shift with increasing temperature in (B). C) The peak potentials derived from the CV scans of $Pd_{0.52}Ag$/CNTs electrocatalysts in panels (A) and (B) plotted vs. the peak current density; D) Peak current density of $Pd_{0.52}Ag$ derived from panel (A) as a function of the light intensity. Alongside, the red dots show the peak potential (right axis) under various light intensities. The dotted blue line is a guide to the eye. The solid blue line represents a linear extrapolation based on the (four) data points acquired at the lowest levels of intensity (0–0.32 Wcm^{-2}). Data points for peak current density represent the average of measurements across three identical trials, the standard deviation of which is represented by the error bars.

Photoexcited or hot e^- generated at the Pd_xAg electrocatalyst by LSPR excitation can be transferred to the external circuit or to e^--accepting adsorbates (Scheme 1).[4g] The hot h^+ left behind in the alloy can participate in MOR through a pathway complementary to electro-oxidation. Hot h^+ significantly deeper in energy, relative to the potential of the working electrode, can be transferred to adsorbed

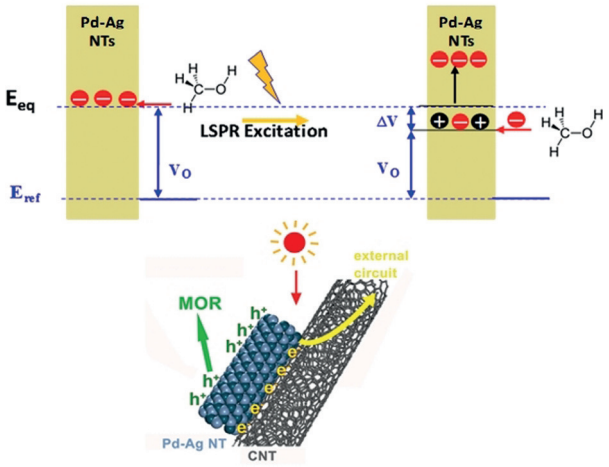

Scheme 1. Top: Energy diagram of Pd_xAg/CNTs electrocatalysts in the dark (left) and under LSPR excitation (right). E_{ref} is the reference potential and E_{eq} represents the equilibrium potential of MOR and V_O is the OCP. LSPR excitation of the electrocatalyst is proposed to generate energetic h^+, leading to a decrease in the OCP by ΔV. e^- are swept into the external circuit. Bottom: Enhanced electrocatalytic MOR activity of CNT-supported Pd_xAg alloy NTs under LSPR excitation.

methanol at a rate much faster than that of h^+ at the applied potential. If h^+ transfer to adsorbed methanol were the rate-limiting process in the electro-oxidation by the Pd_xAg catalyst, then the MOR rate would be enhanced under conditions where hot h^+ transfer is prevalent, resulting in a mass activity enhancement. Thus, at the same applied potential, the depletion in the methanol concentration at the electrode is greater under light illumination as compared to that in the dark. Consequently, a larger concentration gradient is built up between the electrode and the bulk solution and a higher peak current density is attained under light excitation. The higher the light illumination intensity, the deeper in energy, on average, is the hot h^+ distribution generated by LSPR excitation, the faster is the kinetics of h^+ transfer, and the higher is the peak oxidation current. Furthermore, owing to the larger concentration gradient setup under light excitation, the flux of methanol to the electrode reaches its maximum only at a more positive potential as compared to that in the dark. This phenomenon explains the shift in the peak potential observed under LSPR excitation (Figure 3A).

To further characterize the influence of LSPR excitation on the MOR potential, the open-circuit potential (OCP) of $Pd_{0.52}Ag$/CNTs was measured in an aqueous solution of 1.0 M CH_3OH and 0.5 M NaOH under 530 nm laser illumination (Figure 4). In the dark state, the OCP is determined by the difference in the equilibrium potential of methanol oxidation at the $Pd_{0.52}Ag$/CNTs electrode and the reference potential. Under laser illumination, the OCP shifted to a lower steady-state magnitude on the timescale of minutes (Figure 4A). Hot h^+ photogenerated in the $Pd_{0.52}Ag$ NTs under LSPR excitation accumulate over time as e^- are removed to the external circuit aided by the high conductivity of the CNT support (Supporting Information, Figure S6). The reduction in the OCP can be attributed to the consequent lowering of the

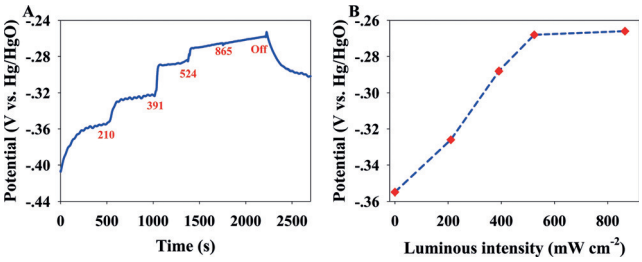

Figure 4. A) The OCP of $Pd_{0.52}Ag$/CNTs electrocatalyst in an aqueous solution of 1.0 M CH_3OH and 0.5 M NaOH measured as a function of time under illumination of various intensities (indicated in $mW cm^{-2}$ at the onset of the illumination condition by the numerical labels in blue) of a 530 nm laser. B) Dependence of the OCP on the incident light intensity. The dashed line is to guide for the eye.

quasi-Fermi level of the alloy under LSPR excitation. The magnitude of the OCP decreased with increasing intensity until the trend reached saturation at an intensity of 524 $mW cm^{-2}$ (Figure 4B). The size of the accumulated hot h^+ population depends on the rate of photogeneration of h^+ relative to the rate of their loss by e^-–h^+ recombination. The former process has a first-order dependence on the excitation intensity, whereas the latter has a second-order dependence on intensity. Therefore, an increase in the light intensity results in an increase in the size of the hot h^+ population, resulting in a larger down-shift of the quasi-Fermi level and therefore of the OCP. At considerably higher light intensity, e^-–h^+ recombination becomes dominant and the size of the hot h^+ population does not increase further with an increase in the light intensity. As a result, the light-intensity-dependent trend of the OCP reaches saturation. It must be noted that the magnitude of the shift of the OCP (ca. 86 mV at 524 $mW cm^{-2}$) upon LSPR excitation is on the order of photoinduced potentials of Au NPs measured under LSPR excitation by Atwater,[5a] Jain,[4f] and Brus[17] labs. The progressive shift with increase in the illumination intensity until a point of saturation is also consistent with these past findings.[4f]

In summary, Pd_xAg alloy NTs synergistically combine the plasmonic attributes of Ag with the electrocatalytic activity of Pd toward MOR, a key fuel cell process. The MOR electrocatalysis of these NTs is modulated by visible-light excitation of LSPRs in the Pd_xAg alloy NTs. Under light, the mass activity of Pd_xAg alloy NTs toward MOR is enhanced, increasingly super-linearly with increasing light intensity. The peak potential for MOR also shifts to more positive potentials under LSPR excitation, which was ascribed to hot h^+-assisted methanol oxidation. The Pd_xAg NTs maintained 89.3% of their activity and a largely stable composition after 6 h of testing under light excitation (Supporting Information, Figure S7). Carbonate and formate were produced under both dark and light excitation conditions (Supporting Information, Figures S8 and S9), but no other gaseous products were detected (Supporting Information, Figure S10). Thus, LSPR excitation has the potential for reducing precious Pd usage in fuel cell catalysts. The plasmonic/electrocatalytic alloys described here may serve as platforms for studying the influence of LSPR excitation on a gamut of electrocatalytic processes.

Acknowledgements

This work was supported by the National Natural Science Foundation of China (No. 51602106) and Guangdong Innovative and Entrepreneurial Research Team Program (No. 2016ZT06N569). P.K.J.'s contribution to interpretation of findings and manuscript writing is supported by the National Science Foundation under Grant NSF CHE-1455011.

Conflict of interest

The authors declare no conflict of interest.

Keywords: electrocatalysis · hot carriers · localized surface plasmon resonance · nanoparticles · palladium–silver alloy

How to cite: *Angew. Chem. Int. Ed.* **2019**, *58*, 8794–8798
Angew. Chem. **2019**, *131*, 8886–8890

[1] a) T. Hirakawa, P. V. Kamat, *J. Am. Chem. Soc.* **2005**, *127*, 3928–3934; b) Z. W. Liu, W. B. Hou, P. Pavaskar, M. Aykol, S. B. Cronin, *Nano Lett.* **2011**, *11*, 1111–1116; c) Y. C. Pu, G. M. Wang, K. D. Chang, Y. C. Ling, Y. K. Lin, B. C. Fitzmorris, C. M. Liu, X. H. Lu, Y. X. Tong, J. Z. Zhang, Y. J. Hsu, Y. Li, *Nano Lett.* **2013**, *13*, 3817–3823.

[2] P. Christopher, H. Xin, A. Marimuthu, S. Linic, *Nat. Mater.* **2012**, *11*, 1044–1050.

[3] a) E. Kazuma, J. Jung, H. Ueba, M. Trenary, Y. Kim, *J. Am. Chem. Soc.* **2017**, *139*, 3115–3121; b) D. F. Swearer, H. Q. Zhao, L. N. Zhou, C. Zhang, H. Robatjazi, J. M. P. Martirez, C. M. Krauter, S. Yazdi, M. J. McClain, E. Ringe, E. A. Carter, P. Nordlander, N. J. Halas, *Proc. Natl. Acad. Sci. USA* **2016**, *113*, 8916–8920; c) H. Huang, L. Zhang, Z. H. Lv, R. Long, C. Zhang, Y. Ling, K. C. Wei, C. M. Wang, L. Chen, Z. Y. Li, Q. Zhang, Y. Luo, Y. J. Xiong, *J. Am. Chem. Soc.* **2016**, *138*, 6822–6828.

[4] a) S. Linic, U. Aslam, C. Boerigter, M. Morabito, *Nat. Mater.* **2015**, *14*, 567–576; b) R. Long, Y. Li, L. Song, Y. J. Xiong, *Small* **2015**, *11*, 3873–3889; c) M. L. Brongersma, N. J. Halas, P. Nordlander, *Nat. Nanotechnol.* **2015**, *10*, 25–34; d) Y. Kim, J. G. Smith, P. K. Jain, *Nat. Chem.* **2018**, *10*, 763–769; e) Y. Kim, A. J. Wilson, P. K. Jain, *ACS Catal.* **2017**, *7*, 4360–4365; f) Y. Kim, D. D. Torres, P. K. Jain, *Nano Lett.* **2016**, *16*, 3399–3407; g) C. H. Choi, K. Chung, T.-T. H. Nguyen, D. H. Kim, *ACS Energy Lett.* **2018**, *3*, 1415–1433.

[5] a) M. T. Sheldon, J. van de Groep, A. M. Brown, A. Polman, H. A. Atwater, *Science* **2014**, *346*, 828–831; b) S. Yu, A. J. Wilson, J. Heo, P. K. Jain, *Nano Lett.* **2018**, *18*, 2189–2194; c) S. Yu, A. J. Wilson, G. Kumari, X. Zhang, P. K. Jain, *ACS Energy Lett.* **2017**, *2*, 2058–2070.

[6] a) L. Cao, F. Scheiba, C. Roth, F. Schweiger, C. Cremers, U. Stimming, H. Fuess, L. Chen, W. Zhu, X. Qiu, *Angew. Chem. Int. Ed.* **2006**, *45*, 5315–5319; *Angew. Chem.* **2006**, *118*, 5441–5445; b) K. Nitul, M. Jatindranath, L. Seok Hee, J. Seung Hyun, V. Balasubramanian, Y. Young Soo, *Chem. Rev.* **2014**, *114*, 12397–12429; c) E. Antolini, *Energy Environ. Sci.* **2009**, *2*, 915–931; d) B. Y. Xia, H. B. Wu, X. Wang, X. W. Lou, *J. Am. Chem. Soc.* **2012**, *134*, 13934–13937.

[7] a) Y. Liu, F. Chen, Q. Wang, J. Wang, J. Wang, T. T. Gebremariam, *J. Mater. Chem. A* **2018**, *6*, 10515 – 10524; b) B. F. Zheng, T. Ouyang, Z. Wang, J. Long, Y. Chen, Z. Q. Liu, *Chem. Commun.* **2018**, *54*, 9583 – 9586; c) H. Xu, P. Song, J. Wang, F. Gao, Y. Zhang, J. Guo, Y. Du, J. Di, *ChemElectroChem* **2018**, *5*, 1191 – 1196; d) H. Xu, P. Song, J. Wang, Y. Shiraishi, Y. Du, Q. Liu, *ACS Sustainable Chem. Eng.* **2018**, *6*, 7159 – 7167; e) H. Yang, Z. H. Wang, Y. Y. Zheng, L. Q. He, C. Zhan, X. Lu, Z. Q. Tian, P. P. Fang, Y. Tong, *J. Am. Chem. Soc.* **2016**, *138*, 16204 – 16207.

[8] Z.-Y. Zhou, N. Tian, Y.-J. Chen, S.-P. Chen, S.-G. Sun, *J. Electroanal. Chem.* **2004**, *573*, 111 – 119.

[9] P. F. Barbieri, A. D. Siervo, M. F. Carazzolle, R. Landers, G. G. Kleiman, *J. Electron Spectrosc. Relat. Phenom.* **2004**, *135*, 113 – 118.

[10] S. K. Sengar, B. R. Mehta, Govind, *J. Appl. Phys.* **2014**, *115*, 124301.

[11] K. Miao, U. Luo, J. Zou, J. Yang, F. Zhang, L. Huang, J. Huang, X. Kang, S. Chen, *Electrochim. Acta* **2017**, *251*, 588 – 594.

[12] Y. J. Xiong, J. Y. Chen, B. Wiley, Y. N. Xia, Y. D. Yin, Z. Y. Li, *Nano Lett.* **2005**, *5*, 1237 – 1242.

[13] a) E. Prodan, C. Radloff, N. J. Halas, P. Nordlander, *Science* **2003**, *302*, 419 – 422; b) Y. Yu, V. Sundaresan, K. A. Willets, *J. Phys. Chem. C* **2018**, *122*, 5040 – 5048; c) X. Zhang, X. Li, D. Zhang, N. Q. Su, W. Yang, H. O. Everitt, J. Liu, *Nat. Commun.* **2017**, *8*, 14542; d) H. Yang, L. Q. He, Y. W. Hu, X. H. Lu, G. R. Li, B. J. Liu, B. Ren, Y. Tong, P. P. Fang, *Angew. Chem. Int. Ed.* **2015**, *54*, 11462 – 11466; *Angew. Chem.* **2015**, *127*, 11624 – 11628.

[14] a) J. G. Smith, J. A. Faucheaux, P. K. Jain, *Nano Today* **2015**, *10*, 67 – 80; b) S. Link, M. A. El-Sayed, *J. Phys. Chem. B* **1999**, *103*, 8410 – 8426.

[15] P. K. Jain, W. Qian, M. A. El-Sayed, *J. Am. Chem. Soc.* **2006**, *128*, 2426 – 2433.

[16] a) N. Wakabayashi, H. Uchida, M. Watanabe, *Electrochem. Solid State* **2002**, *5*, E62 – E65; b) J. L. Cohen, D. J. Volpe, H. D. Abruna, *Phys. Chem. Chem. Phys.* **2007**, *9*, 49 – 77.

[17] X. M. Wu, E. S. Thrall, H. T. Liu, M. Steigerwald, L. Brus, *J. Phys. Chem. C* **2010**, *114*, 12896 – 12899.

Manuscript received: March 16, 2019
Accepted manuscript online: April 30, 2019
Version of record online: May 22, 2019

